Enhanced sub-bandgap efficiency of a solid-state organic intermediate band solar cell using triplet-triplet annihilation†

YunHui L. Lin,[1] Marius Koch,[2] Alyssa N. Brigeman,[3] David M. E. Freeman,[4] Lianfeng Zhao,[1] Hugo Bronstein,[4] Noel C. Giebink,[3] Gregory D. Scholes,[2] Barry P. Rand[1, 5*]

Affiliations:

[1]Department of Electrical Engineering, Princeton University, Princeton, New Jersey 08544, USA

[2]Department of Chemistry, Princeton University, Princeton, New Jersey 08544, USA

[3]Department of Electrical Engineering, The Pennsylvania State University, University Park, Pennsylvania 16802, USA

[4]Department of Chemistry, University College London, London WC1H 0AJ, United Kingdom

[5]Andlinger Center for Energy and the Environment, Princeton University, Princeton, New Jersey 08544, USA

†Electronic supplementary information (ESI) is available: steady-state absorption spectra, additional transient absorption spectra and analysis, x-ray photoelectron spectroscopy, solar cell current-voltage characteristics

*Correspondence to: brand@princeton.edu

Conventional solar cells absorb photons with energy above the bandgap of the active layer while sub-bandgap photons are unharvested. One way to overcome this loss is to capture the low energy light in the triplet state of a molecule capable of undergoing triplet-triplet annihilation (TTA), which pools the energy of two triplet states into one high energy singlet state that can then be utilized. This mechanism underlies the function of an organic intermediate band solar cell (IBSC). Here, we report a solid-state organic IBSC that shows enhanced photocurrent derived from TTA that converts sub-bandgap light into charge carriers. Femtosecond resolution transient absorption spectroscopy and delayed fluorescence spectroscopy provide evidence for the triplet sensitization and upconversion mechanisms, while external quantum efficiency measurements in the presence of a broadband background light demonstrate that sub-bandgap performance enhancements are achievable in this device. The solid-state architecture introduced in this work serves as an alternative to previously demonstrated solution-based IBSCs, and is a compelling model for future research efforts in this area.

BROADER CONTEXT

When applied to solar cells, photochemical upconversion is an attractive technique for harvesting the energy of sub-bandgap photons. By taking better advantage of the full solar spectrum, devices using upconversion can theoretically exceed the Shockley-Queisser limit. To date, most research efforts in this area have invoked a design in which a distinct upconversion layer is positioned external to and at the rear of the device; this upconversion layer serves as an antenna— absorbing low energy photons and re-radiating the upconverted light into the active solar cell for reabsorption. However, optically coupling the upconverted light into the device is often inefficient. In contrast, organic intermediate band solar cells take advantage of *electrically* integrated upconversion, but these remain relatively unexplored. In this report, we demonstrate a solid-state organic intermediate band solar cell, providing proof-of-principle through photophysical analysis and device characterization, and describe directions for future work in this area.

INTRODUCTION

Conventional solar cells are unable to productively harness photons with energy below the bandgap of its active layers. As a result, large swaths of the solar spectrum are wasted, partly accounting for why the maximum theoretical power conversion efficiency (PCE) of conventional solar cells cannot exceed 32% under standard conditions.[1] The intermediate band solar cell (IBSC) concept circumvents this limitation by introducing a narrow band of states within the bandgap of the absorber material that serves as a stepping-stone for the absorption of low energy photons that would have otherwise been lost. While such a device is able to utilize sub-bandgap photons, charges are still extracted via the outer band edges, so that the enhancement in photocurrent due to increased absorption is not achieved at the expense of photovoltage.

To date, demonstrations of IBSC devices are dominated by inorganic semiconductor approaches, in which the intermediate band states are typically achieved by extreme lattice mismatch or dense sheets of quantum dots.[2,3] However, this approach has historically been frustrated by materials limitations and fabrication challenges. Moreover, charge recombination via the intermediate band has proven difficult to avoid. In 2008, the theoretical foundations were laid for an IBSC based on molecular materials and triplet-triplet annihilation upconversion (TTA-UC).[4] It was proposed that the molecular triplet

level of an organic material (the TTA host) serves as the intermediate band. The triplet level of the TTA host is populated indirectly through a sensitization process using a phosphorescent molecule. Subsequently, TTA in the host leads to high energy singlet excitons that can then dissociate via a charge transfer (CT) mechanism wherein holes and electrons are transferred to the donor and acceptor of the solar cell, respectively. Importantly, in order to realize the efficiency gains associated with the IBSC, the CT state of the donor/acceptor interface must be higher in energy than the triplet level of the TTA host. In sum, sub-bandgap photoexcitations in the triplet sensitizer undergo TTA-UC and the resulting singlet excitons dissociate and are extracted as photocurrent across the donor and acceptor layers.

The molecular IBSC is fundamentally different from its inorganic relative in that its intermediate band comprises long-lived (radiatively dark) triplet states rather than a partially-filled band of free carrier states. This difference constitutes a practical advantage for implementing the IBSC because it simplifies the requirement of preventing electrical recombination through the intermediate band since relaxation of triplet excitons to the singlet ground state is spin-forbidden. The limiting PCE of a molecular IBSC with a mid-gap intermediate band is 45.9%,[4,5] which is identical to that of its close relative, the singlet fission solar cell.[6,7] Despite this attractive prediction, the molecular IBSC has not received much attention. Work on TTA-based upconversion solar cells to date have focused on an upconversion layer that is physically separate from the active solar cell.[8-13] In these devices, the upconversion layer absorbs low energy photons, typically at the rear of the device, and re-radiates the high energy photons into the active solar cell for reabsorption. The development of IBSCs with electrically integrated upconversion processes remains in its early stages.

RESULTS AND DISCUSSION

1. Characterization of device energetics

Here we demonstrate a solid-state organic IBSC based on electrically integrated molecular TTA-UC. Until now, the molecular IBSC has been pursued in dye-sensitized architectures where the triplet sensitizer and TTA host are intimately bound or mixed.[14-16] Unlike these, our solid-state device design employs a distinct sensitizer-free “spacer” layer that reduces contact between the site of triplet sensitization and the site of TTA-UC. A

material system consisting of platinum(II) tetraphenyltetrabenzoporphyrin (PtTPBP) as the triplet sensitizer and α-sexithiophene (α-6T) and diindenoperylene (DIP) as donor and acceptor (Fig. 1a), respectively, was strategically selected to meet the energetic requirements of the IBSC. First, the singlet and triplet levels of PtTPBP are nested between those of α-6T (which serves as the TTA host) to enable the triplet sensitization cycle. Second, the α-6T/DIP CT state lies above the triplet level of α-6T in order to constrain photocurrent generation only to α-6T singlet excitons generated by means of TTA-UC (Fig. 1b).

As an experimental control, we perform parallel investigations of a second device, a triplet sensitized solar cell (TSSC).[17,18] In the TSSC, C_{60} is substituted for DIP as the acceptor material, which results in a donor/acceptor CT state that is *lower* in energy than the triplet level of α-6T. Consequently, triplets that are generated in α-6T by the sensitization process are readily dissociated at the donor/acceptor interface, bypassing TTA-UC and contributing directly to photocurrent. This control allows us to distinguish different mechanisms of photocurrent generation in the two types of devices.

The device structure and exciton energy diagrams of the IBSC and TSSC devices are summarized in Fig. 1a & b. The singlet and triplet energies of PtTPBP and α-6T are obtained from literature[19,20] and/or the low energy absorption edge of neat films (ESI† Section 1). There is some uncertainty surrounding the lowest lying triplet level of α-6T, but a value of 1.51 eV is predicted based on trends observed by high-resolution spectroscopy on the delayed fluorescence of solid-state oligothiophenes with chain lengths between 2 and 5.[21,22]

The CT state energies of the α-6T/C_{60} and α-6T/DIP interfaces were characterized by electroluminescence (EL) and external quantum efficiency (EQE) measurements on the relevant interfaces in a device configuration. The EL spectrum of a planar heterojunction α-6T/DIP device is shown in Fig. 1c top, and contains contributions from α-6T and DIP excitons in addition to CT excitons formed at the interface. Emission from CT excitons dominates at low driving voltages.[23,24] The EL spectrum of this interface has been previously deconvolved, with the conclusion that the peak at 1.82 eV is attributable to the CT state.[25] The CT state energy of the α-6T/DIP interface has also been characterized previously by photoelectron spectroscopy and an investigation of the temperature dependence of device open-circuit voltage, with a value of 1.8-1.9 eV reported in either

case.[25,26] The EQE measurement on a planar heterojunction α-6T/C_{60} device is shown in Fig. 1c bottom, and exhibits the characteristic low energy parabolic CT feature when viewed on a semilog scale. Using Marcus theory of photoinduced electron transfer,[27-29] as reported in previous work,[30-32] we determine the CT state energy to be 0.91 eV for the α-6T/C_{60} system. Moreover, the EL spectrum for this system shows emission from low energy CT excitons of similar energy and the value reported in literature, determined from photoelectron spectroscopy, is consistent.[26] As it is critical to TSSC and IBSC device operation, we can conclude that the α-6T triplet energy is above and below the CT state energies of α-6T/C_{60} and α-6T/DIP heterojunctions, respectively.

2. Proof of triplet sensitization and TTA-UC

Pump-probe transient absorption spectroscopy (TAS) is useful in understanding exciton dynamics in the α-6T:PtTPBP host:guest system. As shown in Fig. 2a, isolated PtTPBP molecules in a polystyrene matrix show pronounced absorption bands at 433 and 617 nm with weaker bands at 478, 568, and 670 nm. On the other hand, the neat α-6T film absorbs broadly in the visible spectrum with peaks at 448, 478, and 519 nm (ESI† Section 1). When α-6T is doped with PtTPBP, as shown in Fig. 2d, the absorption spectrum is a superposition of the individual PtTPBP and α-6T spectra with minor band shifts owing to the altered molecular environment in the mixed film. No additional absorption bands are observed at these doping concentrations that would indicate charge transfer transitions. Emission peaks that are related to excimer or exciplex-like species have sometimes been observed,[33] but are absent in our system.

We took advantage of the non-overlapping absorption spectra of PtTPBP and α-6T in the region beyond 600 nm (Fig. S1, ESI†) to selectively excite the PtTPBP molecules. The difference absorption spectra (ΔA) of the isolated PtTPBP and α-6T:PtTPBP(5 wt%) films between 300 fs and 5 ns are shown in Fig. 2b and 2e. Upon excitation at 620 nm, the isolated PtTPBP film shows negative ΔA bands that overlap with the steady-state absorption spectra in Fig. 2a, and are therefore assigned to depopulation of the ground state of PtTPBP, S_0^{Pt}. Intersystem crossing to the first excited triplet state, T_1^{Pt}, takes place within the first picosecond after photoexcitation ($\tau \sim$ 400-500 fs) as determined from global analysis and in agreement with literature.[34] The lifetime of T_1^{Pt} exceeds the experimental time window of our TAS apparatus (~ 7 ns), such that no further changes are

observed in the ΔA spectra after intersystem crossing is complete. Measurements at lower excitation energies (Fig. S2 and S3, ESI†) show a slight deceleration of the T_1^{Pt} decay towards the end of the instrument observation window, pointing towards residual contributions from TTA in the isolated PtTPBP molecules at high excitation energies. Sensitizer-sensitizer TTA is a loss pathway in IBSC devices, but can be mitigated through the solid-state design utilized in this work, because each PtTPBP sensitizer molecule is surrounded by α-6T molecules whose mutual interaction outcompetes the ns-scale TTA process between PtTPBP molecules. The absence of steady-state emission peaks signaling sensitizer aggregation supports this fact.

In the α-6T:PtTPBP(5 wt%) film, intersystem crossing is observed in PtTPBP after excitation at 620 nm and on similar time scales as for the isolated PtTPBP. Importantly, however, the lifetime of T_1^{Pt} is shortened considerably; the transient signals decay almost to zero within the experimental time window. In addition, two spectral modulations are visible— most noticeably at 480 nm but also beyond 700 nm. By comparison with an α-6T reference film and the α-6T:PtTPBP(5 wt%) film excited at 520 nm (Fig. S4, ESI†), these new features are assigned to the ground state depopulation and triplet population of α-6T, respectively (see ESI† Section 2) .

The new ΔA transient above 700 nm, with different shape and constant amplitude between 1 ps and 1 ns in the isolated PtTPBP matrix, resembles the ΔA transient that is visible when exciting α-6T selectively at 520 nm (Fig. S4a, ESI†). Additionally, as mentioned, the transient above 700 nm appears alongside the negative ground state bleach of α-6T, which is best visualized at 480 nm but also present at 448 and 520 nm. Therefore, we can assign the 700 nm transient to an α-6T feature, confirming that the triplet states of α-6T are populated by exciton transfer from the triplet states of PtTPBP. Note that a direct singlet transfer from PtTPBP to α-6T is highly unlikely due to the large energetic barrier (~0.4 eV) and high rate of intersystem crossing in PtTPBP (on the order of 10^{12} s^{-1}). In fact, singlet transfer in the opposite direction, from α-6T to PtTPBP, is the operational pathway and can be seen as a PtTPBP ground state bleach at 620 nm in Fig. S4c (ESI†), suggesting that α-6T singlets are deactivated by neighboring PtTPBP molecules (if present). Therefore, the appearance of the α-6T bleach and triplet transient in Fig. 2e cannot be explained by singlet transfer from PtTPBP to α-6T.

In summary, pump-probe transient absorption experiments with femtosecond time resolution have revealed that when PtTPBP is excited, its triplet lifetime is shortened considerably in the presence of neighboring α-6T molecules as compared to isolated PtTPBP molecules in a polystyrene matrix. Moreover, this shortening of the PtTPBP triplet lifetime is correlated with the ground state depopulation and triplet population of α-6T, thus providing conclusive evidence of triplet exciton transfer between PtTPBP and α-6T, which completes the triplet sensitization cycle.

Following exciton transfer from sensitized PtTPBP molecules, triplets in α-6T undergo TTA-UC to yield high energy singlets. To verify this mechanism, we monitor the power dependence of upconverted fluorescence from α-6T:PtTPBP films. Because TTA-UC is a bimolecular process involving two triplet excitons, the yield of upconverted fluorescence follows the square of the concentration of triplets, which, at the limit of low upconversion efficiency, follows the square of the power density of the incident light.[13,19,35-38] As shown in Fig. 3a, following selective excitation of the PtTPBP chromophores at λ = 633 nm, the film is observed to emit shorter wavelength photons with spectral shape identical to that of α-6T, verifying that upconversion to α-6T singlets has taken place. In contrast, a pure α-6T film exhibited no such emission when excited under identical conditions. Moreover, in the sensitized film, a log-log plot of the integrated upconverted fluorescence intensity versus the incident power density at 633 nm reveals a slope of 2, which reflects the bimolecular nature of TTA-UC (Fig. 3c). On the other hand, when the film is excited at λ = 405 nm, which directly excites the α-6T singlet manifold (Fig. 3b), the power dependence is linear (Fig. 3c). Taken together, these results highlight the mechanistic differences in fluorescence originating from α-6T versus PtTPBP sites, and provide conclusive evidence of the triplet sensitization and upconversion processes that underlie molecular IBSCs.

At the limit of low TTA-UC efficiency, the α-6T triplet decay is dominated by first-order decay channels (e.g. non-radiative losses), such that the triplet population is related linearly to the excitation power density. Consequently, the delayed fluorescence of α-6T is expected to vary quadratically with the excitation flux ($[S_1] \propto [T_1]^2 \propto \text{Flux}^2$). However, at the limit of high TTA-UC efficiency, TTA-UC outcompetes first-order decay channels such

that the α-6T triplet population is now related to the square root of the excitation flux, and the delayed fluorescence of α-6T is expected to vary linearly with the excitation power density ($[S_1] \propto [T_1]^2 \propto (\sqrt{Flux})^2$. The threshold power density at which the system transitions between low and high TTA-UC efficiency regimes is an important metric for evaluating the overall performance of devices using TTA-UC,[37] and should be pursued in future iterations of the IBSC.

3. Demonstration of photocurrent enhancement due to TTA-UC

To complement the spectroscopic evidence for triplet sensitization and TTA-UC in an α-6T:PtTPBP system, we perform comparative studies of photocurrent generation in the IBSC and TSSC device systems as a function of the α-6T layer thickness and as a function of background light intensity. Both experiments are designed to modulate the likelihood of TTA-UC, which enhances sub-bandgap photocurrent generation in the IBSC devices but detracts from it in the TSSC control devices.

As shown in Fig. 1a, the IBSC and TSSC devices were fabricated with a 50 nm α-6T layer doped with PtTPBP followed by an undoped α-6T “spacer" layer, deposited with thicknesses between 0 and 65 nm in 5 nm increments. The motivation behind this neat α-6T spacer is to help separate the site of α-6T triplet sensitization from the site of TTA-UC, thereby reducing the chance of counterproductive back-transfer of upconverted α-6T singlets to PtTPBP (as encountered in the spectroscopy measurements of Fig. S4c, ESI†). To confirm the spacer structure, depth-resolved x-ray photoelectron spectroscopy showed that an α-6T spacer achieves complete coverage over the α-6T:PtTPBP (5 wt%) film within only a couple of nm (ESI† Section 3).

The triplets of α-6T are reported to have a relatively long lifetime of 24 μs in solution,[39] such that introducing a neat α-6T spacer layer provides opportunities for upconversion interactions between long-lived, diffusive triplets without competition from quenching processes on sensitizer sites. However, the thicker the spacer layer, the more diluted the triplets become and the less efficiently excitons diffuse to the dissociating donor/acceptor interface, such that we expect an optimum spacer thickness to exist when triplet-triplet interactions are maximized with respect to the exciton diffusion efficiency. If a different material were to be incorporated as the sensitizer-free spacer layer that

possesses a triplet energy slightly lower than that of the sensitizer host, then the sensitized triplets can be driven energetically into the spacer layer, thus counteracting the triplet dilution effect encountered in the case where the sensitizer host and spacer materials are identical.

As seen in the exciton energy diagrams in Fig. 1b, in the IBSC, TTA-UC enables the harvesting of α-6T triplets whose energy can be used towards populating CT states instead of being wasted. In the TSSC, however, TTA-UC is a loss process because for each pair of α-6T triplets that could have previously populated two CT states, instead only one CT state is populated by the resulting singlet, with more than 1 eV excess energy lost as heat. Because of these contrasting behaviors, studying the change in photocurrent generation under different degrees of TTA-UC in these two devices presents a unique opportunity to confirm the functionality of an IBSC device.

The current-voltage characteristics of the IBSC and TSSC devices were measured in dark and 1 sun conditions, with results shown in ESI† Section 4. It is noteworthy that the presence of the PtTPBP sensitizer does not affect the open-circuit voltage (V_{OC}) of either the IBSC or TSSC devices. This is an encouraging sign that PtTPBP, which has a nearly resonant highest occupied molecular orbital (4.9 eV)[40] compared to α-6T (4.85 eV),[41] does not act as a hole trap. It also implies that the introduction of intermediate PtTPBP triplet states does not interfere with charge extraction via the α-6T band edges. In the current-voltage data, we also observe a positive trend in device short-circuit current (J_{SC}) as a function of spacer thickness for IBSCs and a negative trend for TSSCs. While we recognize that broadband photocurrent generation in these devices is affected by many variables (e.g. amount of light absorption, thin-film interference, differences in exciton diffusion), the fact that the trends are opposite for each series of devices is nevertheless revealing. Given that both IBSC and TSSC devices were fabricated with nominally identical α-6T:PtTPBP and subsequent α-6T spacer layers, absorption and exciton diffusion characteristics within the donor layer should be similar for both series of devices. The J_{SC} under broadband 1 sun illumination is dominated by α-6T singlet absorption, but these singlets are subject to triplet sensitization via nearby PtTPBP sites, and have the opportunity to undergo TTA-UC with other triplets. The likelihood of these annihilating encounters increases (at least initially) in devices with a high volume of α-6T (i.e. large spacer) and is therefore consistent with the opposite

trends observed in the J_{SC} of IBSC and TSSC devices. At the largest spacer thicknesses, reduced exciton diffusion efficiency may override the effects of increased TTA-UC, such that the photocurrent response plateaus.

As another method of modulating the degree of TTA-UC in these devices, we performed EQE measurements in the presence of a background white light (Fig. 4).[42] In these measurements, the EQE of each device was measured using conventional lock-in detection techniques involving a chopped monochromatic source and an unchopped background light, thereby limiting our study to interactions between excitons originating from the monochromatic and background beams. Changes in the locked-in signal may therefore be linked to the presence of higher concentrations of background excitons (or polarons) in the device. Because the background light is broadband, it is able to excite α-6T singlet excitons, which can then undergo the sensitization process through PtTPBP to yield α-6T triplets.

The EQE spectra of select IBSC and TSSC devices with (dashed) and without (solid) the background light are shown in Fig. 4d & e around the region of selective PtTPBP excitation. As reasoned earlier, direct excitations on the PtTPBP are sub-bandgap absorption events that cannot be directly collected by the IBSC. In line with our expectations, the IBSC and TSSC show markedly different behaviors in the presence of the background light: the IBSC experiences an enhancement in photocurrent generation while the TSSC experiences a reduction. The magnitude of these enhancements and reductions in the 615 nm EQE response, shown in Fig. 4d & e, are on the order of several percent (see also, Fig. 5a).

Plotted in Fig. 5a is the percentage change in device EQE under constant background light bias at the peak of PtTPBP absorption (615 nm) as a function of the α-6T spacer thickness. In the IBSC, the maximum enhancement in photocurrent was achieved in a device with a 20 nm spacer layer, although a broad optimum exists between 15 and 40 nm. The eventual drop-off in the enhancement at large spacer thicknesses likely reflects a tradeoff between TTA-UC efficiency and exciton diffusion efficiency to the dissociating interface. In the TSSC, the maximum reduction in photocurrent was observed in a device with a 25 nm spacer layer.

An additional study was conducted to observe how the photocurrent response of these two devices evolved under different background light intensities, with results shown in Fig. 5b. In the presence of a background white light, the IBSC experiences a rapid enhancement in photocurrent generation at low background light intensities, peaking at 12% relative photocurrent enhancement under a background intensity less than 0.1 mW/cm^2. Eventually, however, there is a gradual drop-off as the background light intensity is increased further. One possibility for this loss in performance is the presence of exciton-polaron annihilation (EPA), which dominates at higher background intensities. To test this theory, the intensity-dependent measurements were repeated while the IBSC device was kept at a moderate forward or reverse voltage bias. Under a reverse voltage bias, polarons are rapidly swept out of the device, therefore reducing their chance of interaction with the excitons being probed by the EQE measurement. On the other hand, a forward voltage bias inhibits the extraction of polarons, providing greater opportunity for EPA. The data shown in Fig. 5b confirm our theory, with the IBSC under reverse bias experiencing less of a drop-off in performance at high background intensities and the IBSC under forward bias experiencing a more severe drop-off compared to the unbiased case. Moreover, the performance at low background intensities is largely unaffected, suggesting that EPA is only a major influence under high polaron concentrations.

In summary, when conditions are favorable for TTA-UC, we see enhancements in sub-bandgap photocurrent generation in the IBSC while the TSSC shows the opposite behavior. These contrasting behaviors are consistent with the fact that the CT state of the IBSC device is higher in energy than the α-6T triplet, such that optical excitations resulting in triplets can only lead to photocurrent by passing through the TTA-UC process. On the other hand, the CT state of the TSSC device is lower than the α-6T triplet, such that TTA-UC presents a loss mechanism for photocurrent.

4. Directions for future work

While we are able to demonstrate strong evidence that an α-6T:PtTPBP/DIP system functions as an organic IBSC, our work, along with that of other researchers,[43-45] has also allowed us to identify directions for future work to boost their performance. To evaluate the limitations of a particular system, we break down the EQE of an organic IBSC at the

wavelength of selective sensitizer excitation (in our case, 615 nm) into several sequential processes:

$$EQE(615\,nm) = \eta_{abs}\eta_{TS}\eta_{TTA}\eta_{ED}\eta_{CT}\eta_{CC}$$

where η_{abs} is the absorption efficiency, η_{TS} is the efficiency of the triplet sensitization process, η_{TTA} is the probability that an α-6T triplet undergoes TTA-UC to yield a high energy singlet, η_{ED} is the exciton diffusion efficiency, η_{CT} is the charge transfer efficiency, and η_{CC} is the charge collection efficiency.

In our material system, the absorption efficiency at 615 nm, η_{abs}, was estimated by comparing the reflection difference between a neat α-6T/DIP device and a PtTPBP-doped α-6T/DIP device with the same layer structure. The measured reflection difference of 8% approximates the absorption of the PtTPBP sensitizer alone. Improving this value by developing near-infrared triplet sensitizers with high oscillator strength is therefore critical to future progress in this field.

The next step following sub-bandgap excitation is triplet sensitization, an energetically downhill process that can occur with very high efficiency. In fact, many heavy metal porphyrins and phthalocyanines, including PtTPBP, have intersystem crossing yields approaching 100%.[44-46] However, the energy loss in transforming from singlet to triplet (0.2 eV in PtTPBP) is an undesirable side-effect that should be reduced in future iterations of the molecular IBSC.

The TTA-UC efficiency, η_{TTA}, is dictated by spin statistics and the energetic accessibility of different outcomes of the encounter complex between two triplets. Foremost, to encourage efficient, slightly exothermic TTA-UC, the triplet energy of the upconversion material should be just slightly over half that of the singlet. However, the energies of other excited species are also relevant if one is to avoid upconversion to non-singlet species. For the vast majority of TTA host materials, the monomolecular quintet state is too high in energy compared to that of the triplet pair, such that the encounter complex must dissociate back to the monomolecular states.[43-47] In α-6T however, the higher energy triplet T_n may be accessible by absorbing less than 200 meV of energy,[48] resulting in upconversion to the T_n state followed by rapid internal conversion to T_1, recycling one of the original triplets. Assuming both the S_1 and T_n channels are energetically accessible to the triplet encounter complex, the maximum probability that an

individual α-6T triplet ultimately contributes to singlet upconversion is 20%.[43,45,47] The yield of the upconversion process can be boosted even higher by selecting an upconversion material for which both the higher energy triplet and quintet states are energetically inaccessible. This leaves only the singlet channel open for annihilation events, giving a maximum singlet upconversion yield of 50% for each triplet exciton. In addition to these energetic considerations, the ideal upconversion material possesses a high triplet natural lifetime, such that TTA-UC outcompetes other non-radiative triplet decay pathways. This allows TTA-UC to become the dominant triplet decay channel at lower sub-bandgap excitation intensities that are in-line with standard illumination conditions.[36,37] Finally, as discussed earlier, the TTA-UC efficiency can be enhanced significantly by incorporating an upconversion material that is distinct from that which functions as the sensitizer host. The upconversion material should have a triplet energy lower than that of the sensitizer host, in order to drive triplets energetically onto TTA-UC sites and prevent back-transfer, but only *slightly* lower so as to avoid excessive energy loss.

Evaluating the efficiency of the next three processes— exciton diffusion, charge transfer, and charge collection— can be a challenge in complex, multi-layered device systems like a solid-state organic IBSC. However, our EQE experiments revealed that EPA presents a significant loss pathway for sub-bandgap photocurrent at high polaron concentrations, reducing the exciton diffusion efficiency, η_{ED}. One way to combat this is through the judicious selection of organic materials and electrical contacts. In principle, one can engineer an electric field profile that reduces polaron buildup at interfaces.[49,50] Additionally, accelerating exciton and polaron transport through the device is important for reducing annihilating interactions between the two species. In this regard, a solid-state design is well suited for independently optimizing the morphologies (and thus the transport properties) of different device components. Optimizing the efficiency of charge transfer, η_{CT}, requires careful balance between two energetic considerations: on the one hand, increasing the energy gap between the highest occupied molecular orbitals (HOMOs) or lowest unoccupied molecular orbitals (LUMOs) of the donor and acceptor provides greater energetic driving force for charge dissociation, but on the other hand, the energy gap between the donor HOMO and acceptor LUMO must be sufficiently large to bring about a donor/acceptor CT state that is higher in energy than the triplet level of the TTA host.

Overall, our demonstration of a solid-state IBSC showing appreciable sub-bandgap photocurrent is encouraging, but significant materials engineering efforts are needed to bring the sub-bandgap EQE closer to its maximum attainable value.

CONCLUSIONS

In summary, we have developed a solid-state organic IBSC and presented a comprehensive body of evidence supporting its functionality. Transient absorption spectroscopy proved that absorption events on PtTPBP molecules lead to population of α-6T triplets, while delayed fluorescence spectroscopy exhibited the characteristic quadratic power dependence of α-6T emission under selective PtTPBP excitation, confirming that TTA-UC is active in this system. The EQE spectra of IBSC devices showed sub-bandgap photocurrent contributions which were enhanced in the presence of a background light, providing further support for upconversion activity. While leaving significant room for improvement, our demonstration of a solid-state organic IBSC with appreciable sub-bandgap photocurrent generation is an encouraging result that proves molecular IBSCs are a compelling device concept for overcoming conventional efficiency limits.

METHODS

Device Fabrication. Organic materials were purchased from commercial vendors and purified by thermal gradient sublimation prior to use. PtTPBP was synthesized using a procedure described previously[40] and used without further purification. Samples used for spectroscopy were fabricated on clean quartz substrates while samples used for device studies were fabricated on clean patterned indium tin oxide (ITO) substrates, upon which low conductivity poly(3,4-ethylenedioxythiophene):polystyrene sulfonate (PEDOT:PSS) (Heraeus Clevios P VP AI 4083) was spin-coated in ambient air and annealed at 110 °C for 10 min. Organic films and aluminum top-contacts were deposited by vacuum thermal evaporation. Doping was achieved by coevaporation of the PtTPBP and α-6T from two sources with independent deposition rate monitors. The area of each device was 0.1 cm^2. All samples were encapsulated in a dry N_2 environment using a glass (for devices) or quartz (for spectroscopy samples) cover and solvent-free epoxy.

Device Characterization. External quantum efficiency measurements were performed using a Newport TLS-300X tunable light source system. Device spectral response was measured under short-circuit conditions using a Stanford Research Systems

SR570 current pre-amplifier and SR830 lock-in amplifier. A calibrated Newport Si photodiode served as the reference. Background white light was provided by a set of standard 5 mm LEDs with a diffuser to improve uniformity. In these measurements, the EQE of each device was measured using conventional lock-in detection techniques involving a chopped monochromatic source and an unchopped background light, thereby limiting our study to interactions between excitons originating from the monochromatic and background beams.[42] For EQE scans performed in the presence of the background white light, each "light" scan was compared against a "dark" scan performed immediately before under otherwise identical conditions, in order to exclude drift in the signal over time. For voltage bias measurements shown in Fig. 5b, the voltage was provided by the SR570 current pre-amplifier and was applied to both "light" and "dark" scans. Electroluminescence (EL) spectra were measured under constant current bias (5 mA/cm^2 for the α-6T/DIP device and 1.6 A/cm^2 for the α-6T/C_{60} device) using a Horiba fibre-coupled spectrograph with a Si CCD array cooled to -60 °C (for the α-6T/DIP device) and an InGaAs array cooled to -100 °C (for the α-6T/C_{60} device). All measurements were calibrated using an Ocean Optics LS-1 tungsten halogen light source.

Steady-State and Transient Spectroscopy. Absorption spectra were recorded on an Agilent Cary 60 UV-Vis spectrophotometer and Horiba PTI QuantaMaster 400 spectrofluorometer. The absorption of the films was 0.08 at 520 nm for α-6T, and 0.03 and 0.08 at 620 nm for α-6T:PtTPBP and polystyrene:PtTPBP, respectively.

Femtosecond transient absorption spectra were recorded using a Helios transient absorption spectrometer (Ultrafast Systems), with additional experimental details presented in ESI† Section 2. Measurements were conducted at magic angle with beam diameters on the sample around 310 μm at 620 nm, around 1000 μm at 520 nm (note that an imperfect beam shape in the particular experiments done at this wavelength allows only a rough approximation of the value) and 130 μm for the white light probe. The excitation energy was varied between 12.5 and 100 nJ at 620 nm giving a fluence of ~0.016 to 0.13 mJ/cm^2 with a linear dependence of the signal intensity as a function of the excitation energy. The pulse energies resulted in an excitation density on the order of 6 x 10^{17} to 6 x 10^{18} photons/cm^3 for the 50 nm thick α-6T:PtTPBP(5 wt%) film.[51] The irradiance at 520 nm was 150 μW, giving a fluence of approximately 0.019 mJ/cm^2.

Global analysis was performed using a procedure described in literature.[52] Briefly, signal amplitudes in the entire wavelength range were analyzed globally starting from 0.25 ps after optical excitation to avoid contributions from artifacts due to pump-probe overlap. Additionally, no deconvolution of the data with the instrument response function was necessary. To satisfactorily reproduce the experimental data, 3 to 5 time constants were used that had been obtained from a nonlinear least squares fit procedure.

Delayed fluorescence spectroscopy was performed using a Horiba iHR fibre-coupled spectrometer and Si CCD array. A 633 nm HeNe laser and a 405 nm diode laser were used as excitation sources. Incident intensity was tuned over several orders of magnitude using neutral density filters and measured with a calibrated Thorlabs Si photodiode.

REFERENCES

1. W. Shockley, and H. J. Queisser, *J. Appl. Phys.,* 1961*,* **32**, 510-519.
2. A. Luque, A. Martí and C. Stanley, *Nat. Photon*, 2012*,* **6**, 146-152.
3. Y. Okada, N. J. Ekins-Daukes, T. Kita, R. Tamaki, M. Yoshida, A. Pusch, O. Hess, C. C. Phillips, D. J. Farrell, K. Yoshida, N. Ahsan, Y. Shoji, T. Sogabe and J.-F. Guillemoles, *Appl. Phys. Rev*., 2015, **2**, 021302.
4. N. J. Ekins-Daukes and T. W. Schmidt, *Appl. Phys. Lett*., 2008, **93**, 063507.
5. M. J. Y. Tayebjee, D. R. McCamey and T. W. Schmidt, *J. Phys. Chem. Lett.*, 2015, **6**, 2367-2378.
6. M. C. Hanna and A. J. Nozik, *J. Appl. Phys*., 2006, **100**, 074510.
7. M. J. Y. Tayebjee, A. A. Gray-Weale and T. W. Schmidt, *J. Phys. Chem. Lett.*, 2012, **3**, 2749-2754.
8. G.-B. Shan and G. P. Demopoulos, *Adv. Mater*., 2010, **22**, 4373-4377.
9. Y. Y. Cheng, B. Fückel, R. W. MacQueen, T. Khoury, R. G. C. R. Clady, T. F. Schulze, N. J. Ekins-Daukes, M. J. Crossley, B. Stannowski, K. Lips and T. W. Schmidt, *Energy Environ. Sci*., 2012**, 5**, 6953-6959.
10. T. F. Schulze, J. Czolk, Y. Cheng, B. Fückel, R. W. MacQueen, T. Khoury, M. J. Crossley, B. Stannowski, K. Lips, U. Lemmer, A. Colsmann and T. W. Schmidt, *J. Phys. Chem. C*, 2012, **116**, 22794-22801.
11. A. Nattestad, Y. Y. Cheng, R. W. MacQueen, T. F. Schulze, F. W. Thompson, A. J. Mozer, B. Fückel, T. Khoury, M. J. Crossley, K. Lips, G. G. Wallace and T. W. Schmidt, *J. Phys. Chem. Lett*., 2013, **4**, 2073-2078.
12. A. Monguzzi, S. M. Borisov, J. Pedrini, I. Klimant, M. Salvalaggio, P. Biagini, F. Melchiorre, C. Lelii, F. Meinardi, *Adv. Funct. Mater.*, 2015, **25**, 5617-5624.

13. M. Wu, D. N. Congreve, M. W. B. Wilson, J. Jean, N. Geva, M. Welborn, T. Van Voorhis, V. Bulović, M. G. Bawendi and M. A. Baldo, *Nat. Photon*., 2016, **10**, 31-34.
14. C. Simpson, T. M. Clarke, R. W. MacQueen, Y. Y. Cheng, A. J. Trevitt, A. J. Mozer, P. Wagner, T. W. Schmidt and A. Nattestad, *Phys. Chem. Chem. Phys*., 2015, **17**, 24826-24830.
15. S. P. Hill, T. Banerjee, T. Dilbeck and K. Hanson*, J. Phys. Chem. Lett*., 2015, **6**, 4510-4517.
16. S. P. Hill, T. Dilbeck, E. Baduell and K. Hanson, *ACS Energy Lett*., 2016, **1**, 3-8.
17. B. P. Rand, S. Schols, D. Cheyns, H. Gommans, C. Girotto, J. Genoe, P. Heremans and J. Poortmans, *Org. Electron.*, 2009, **10**, 1015-1019.
18. W. A. Luhman and R. J. Holmes, *Appl. Phys. Lett*., 2009, **94**, 153304.
19. T. N. Singh-Rachford and F. N. Castellano, *J. Phys. Chem. Lett*., 2010, **1**, 195-200.
20. D. Beljonne, J. Cornil, R. H. Friend, R. A. J. Janssen and J. L. Brédas, *J. Am. Chem. Soc*., 1996, **118**, 6453-6461.
21. P. Landwehr, H. Port and H. C. Wolf, *Chem. Phys. Lett.,* 1996, **260**, 125-129.
22. C. Taliani and W. Gebauer, in *Handbook of oligo- and polythiophenes*, ed. D. Fichou, WILEY-VCH, Weinheim, 1999, Ch. 7, pp. 361-404.
23. K. Tvingstedt, K. Vandewal, A. Gadisa, F. Zhang, J. Manca and O. Inganäs, *J. Am. Chem. Soc.,* 2009, **131**, 11819-11824.
24. Y. Zhou, K. Tvingstedt, F. Zhang, C. Du, W.-X. Ni, M. R. Andersson and O. Inganäs, *Adv. Funct. Mater*, 2009, **19**, 3293-3299.
25. T. Linderl, U. Hörmann, S. Beratz, M. Gruber, S. Grob, A. Hofmann and W. Brütting, *J. Opt*., 2016, **18**, 024007.
26. A. Wilke, J. Endres, U. Hörmann, J. Niederhausen, R. Schlesinger, J. Frisch, P. Amsalem, J. Wagner, M. Gruber, A. Optiz, A. Vollmer, W. Brütting, A. Kahn and N. Koch, *Appl. Phys. Lett.,* 2012, **101**, 233301.
27. R. A. Marcus, *J. Chem. Phys.*, 1956, **24**, 966-978.
28. I. R. Gould, D. Noukakis, L. Gomez-Jahn, R. H. Young, J. L. Goodman and S. Farid, *Chem. Phys.*, 1993, **176**, 439-456.
29. T. M. Clarke and J. R. Durrant, *Chem. Rev.,* 2010, **110**, 6736-6767.
30. K. Vandewal, K. Tvingstedt, A. Gadisa, O. Inganäs and J. V. Manca, *Phys. Rev. B*, 2010, **81**, 125204.
31. K. R. Graham, P. Erwin, D. Nordlund, K. Vandewal, R. Li, G. O. Ngongang Ndjawa, E. T. Hoke, A. Salleo, M. E. Thompson, M. D. McGehee and A. Amassian, *Adv. Mater*., 2013, **25**, 6076-6082
32. B. Bernardo, D. Cheyns, B. Verreet, R. D. Schaller, B. P. Rand and N. C. Giebink, *Nat. Comm.*, 2014, **5**, 3245.
33. M. D. Perez, C. Borek, P. I. Djurovich, E. I. Mayo, R. R. Lunt, S. R. Forrest and M. E. Thompson, *Adv. Mater*., 2009, **21**, 1517-1520.

34. S. T. Roberts, C. W. Schlenker, V. Barlier, R. E. McAnally, Y. Zhang, J. N. Mastron, M. E. Thompson and S. E. Bradford, *J. Phys. Chem. Lett.*, 2011, **2**, 48-54.
35. R. R. Islangulov, J. Lott, C. Weder and F. N. Castellano, *J. Am. Chem. Soc.*, 2007, **129**, 12652-12653.
36. Y. Y. Cheng, T. Khoury, R. G. C. R. Clady, M. J. Y. Tayebjee, N. J. Ekins-Daukes, M. J. Crossley and T. W. Schmidt, *Phys. Chem. Chem. Phys.*, 2010, **12**, 66-71.
37. A. Haefele, J. Blumhoff, R. S. Khnayzer and F. N. Castellano*, J. Phys. Chem. Lett.*, 2012, **3**, 299-303.
38. P. Mahato, A. Monguzzi, N. Yanai, T. Yamada, and N. Kimizuka, *Nat. Mater.*, 2015, **14**, 924-930.
39. V. Wintgens, P. Valat and F. Garnier,*. J. Phys. Chem.*, 1994, **98**, 228-232.
40. C. Borek, K. Hanson, P. I. Djurovich, M. E. Thompson, K. Aznavour, R. Bau, Y. Sun, S. R. Forrest, J. Brooks, L. Michalski and J. Brown, *Angew. Chem. Int. Ed.*, 2007, **46**, 1109-1112.
41. J. Endres, I. Pelczer, B. P. Rand and A. Kahn, *Chem. Mater.*, 2016, **28**, 794-801.
42. Y. L. Lin, M. A. Fusella, O. V. Kozlov, X. Lin, A. Kahn, M. S. Pshenichnikov and B. P. Rand, *Adv. Funct. Mater.*, 2016, **26**, 6489-6294.
43. T. F. Schulze and T. W. Schmidt, *Energy Environ. Sci*, 2015,*.* **8**, 103-125.
44. J. Zhao, S. Ji and H. Guo, *RCS Adv*., 2011, **1**, 937-950.
45. Y. C. Simon and C. Weder, *J. Mater. Chem.*, 2012, **22**, 20817-20830.
46. T. N. Singh-Rachford and F. N. Castellano, *Coord. Chem. Rev.*, 2010, **254**, 2560-2573.
47. Y. Y. Cheng, B. Fückel, T. Khoury, R. G. C. R. Clady, M. J. Y. Tayebjee, N. J. Ekins-Daukes, M. J. Crossley and T. W. Schmidt, *J. Phys. Chem. Lett.*, 2010, **1**, 1795-1799.
48. R. A. J. Janssen, D. Moses and N. S. Sariciftci, *J. Chem. Phys.*, 1994, **101**, 9519-9527.
49. B. Verreet, P. E. Malinowski, B. Niesen, D. Cheyns, P. Heremans, A. Stesmans and B. P. Rand, *Appl. Phys. Lett.*, 2013, **102**, 043301.
50. B. Verreet, A. Bhoolokam, A. Brigeman, R. Dhanker, D. Cheyns, P. Heremans, A. Stesmans, N. C. Giebink and B. P. Rand, *Phys. Rev. B*, 2014, **90**, 115304.
51. A. A. Paraecattil, S. Beaupré, M. Leclerc, J.-E. Moser and N. Banerji, *J. Phys. Chem. Lett.*, 2012, **3**, 2952-2958.
52. P. Fita, E. Luzina, T. Dziembowska, C. Radzewicz and A. Grabowska, *J. Chem. Phys.*, 2006, **125**, 184508.

ACKNOWLEDGEMENTS

This work was supported by the U.S. Department of Energy, Office of Basic Energy Sciences, Division of Materials Sciences and Engineering under Award Nos. DE-SC0012458 (B.P.R.) and DE-0012365 (N.C.G.), and the Division of Chemical Sciences, Geosciences, and

Biosciences under Award No. DE-SC0015429 (G.D.S.), and the National Science Foundation Award No. CBET-1604524 (B.P.R.). M.K. acknowledges support from a Swiss National Science Foundation postdoctoral fellowship and thanks Dr. Ryan D. Pensack for useful discussions regarding triplet-triplet annihilation.

COMPETING FINANCIAL INTERESTS

The authors declare no competing financial interests.

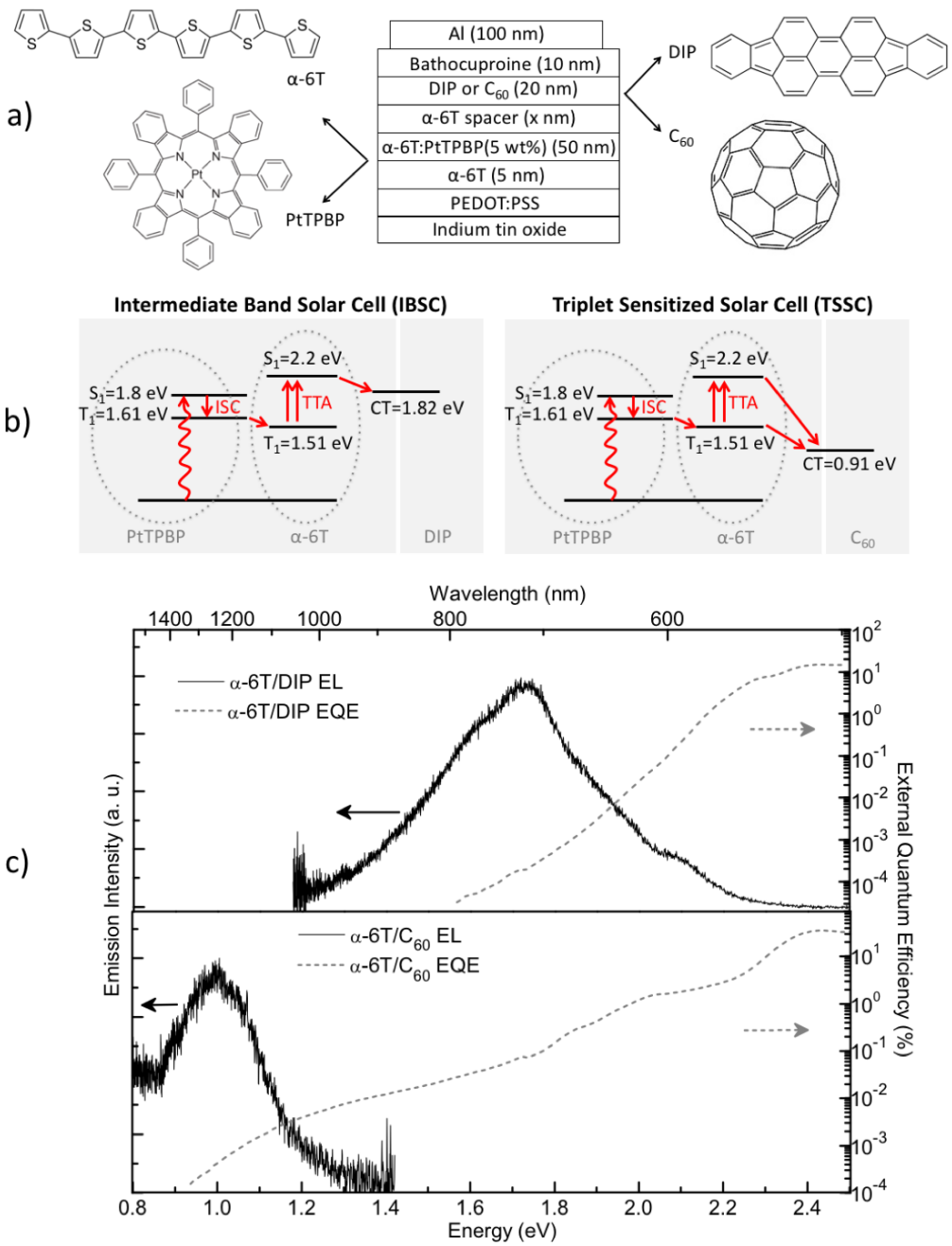

Figure 1. (a) Device structure of the intermediate band solar cell (IBSC) and triplet sensitized solar cell (TSSC). Molecules shown are α-sexithiophene (α-6T), diindenoperylene (DIP), platinum(II) tetraphenyltetrabenzoporphyrin (PtTPBP), and fullerene C_{60}. **(b)** Exciton energy diagrams of the IBSC and TSSC. **(c)** Electroluminescence (EL) and external quantum efficiency (EQE) of the IBSC and TSSC devices, which were used to characterize the charge transfer (CT) state energy of the donor/acceptor interfaces.

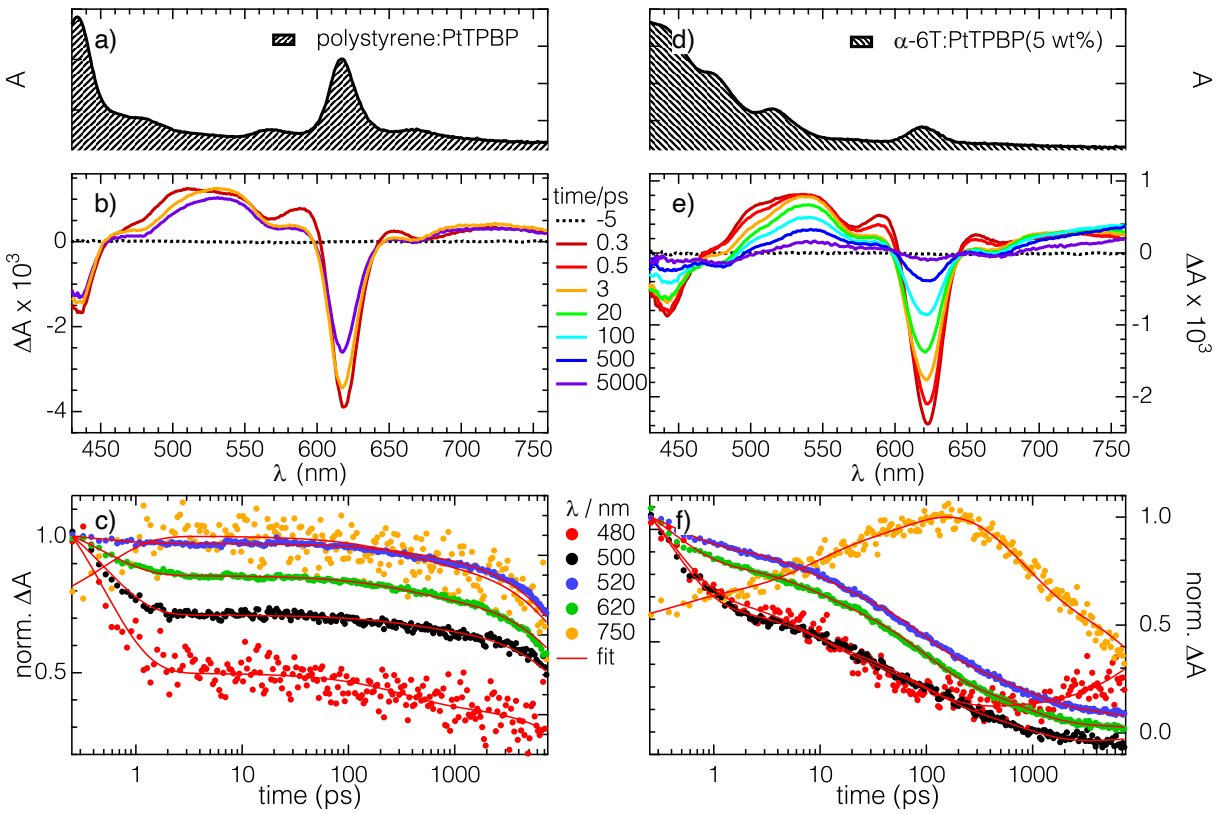

Figure 2. Steady-state absorption spectra of **(a)** isolated PtTPBP in polystyrene matrix and **(d)** an α-6T:PtTPBP(5 wt%) film. In **(b)** and **(e)**, transient absorption spectra (TAS) of the two films recorded after excitation at 620 nm. The excitation energy was 100 nJ per pulse, corresponding to a fluence of roughly 0.13 mJ/cm^2. In **(c)** and **(f)**, the time evolution of the transient amplitudes at select wavelengths (center legend) are shown. Thin red lines represent fits to three **(c)** and five **(f)** exponentials to the experimental data, derived from a global analysis of the entire data set. For better visualization, the negative bleach amplitudes at 620 nm are inverted and the amplitude at 480 nm in **(f)** is adjusted prior to normalization due to its change in sign.

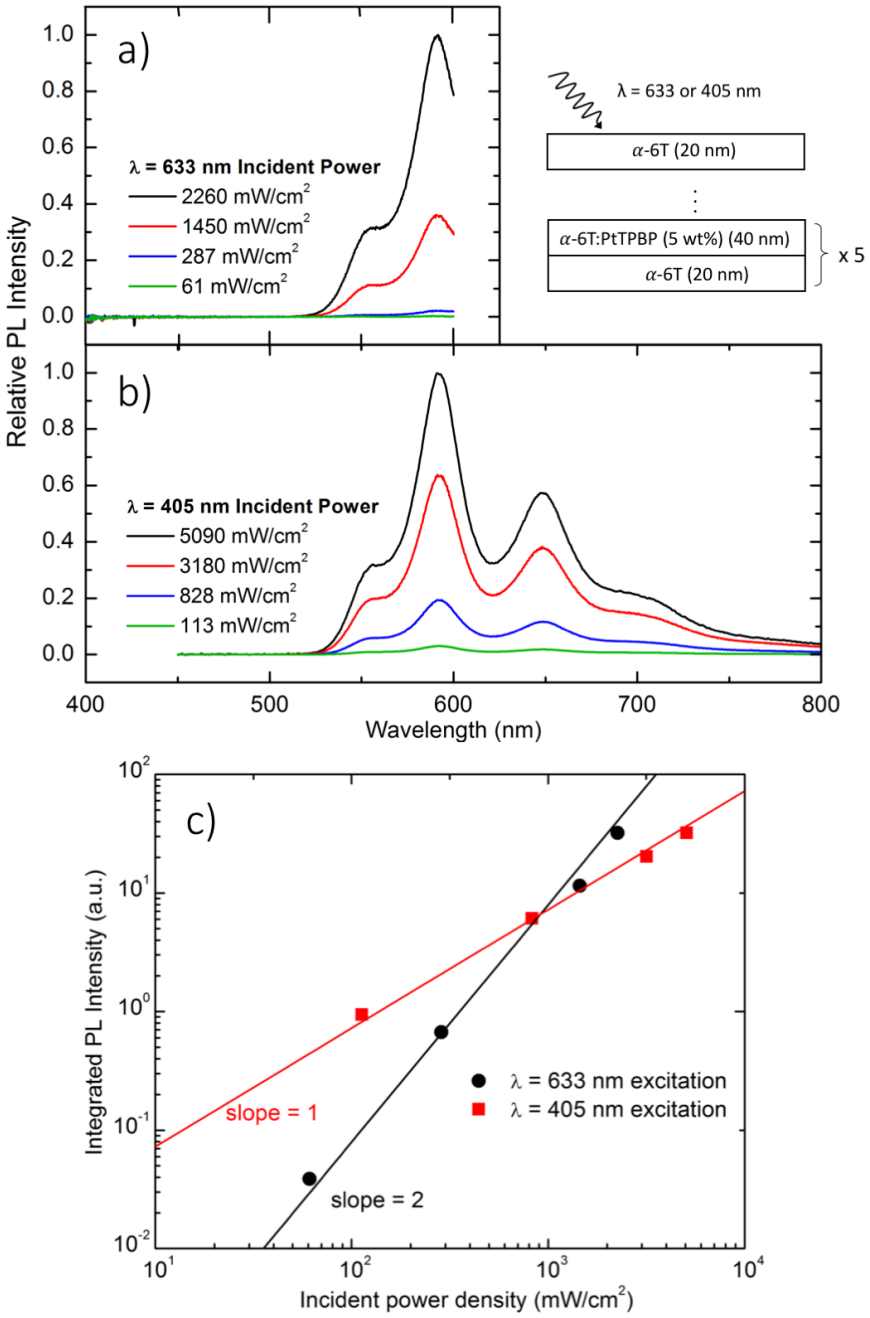

Figure 3. Photoluminescence (PL) of an α-6T film with PtTPBP sensitizer following excitation at λ = 633 or 405 nm. The full film structure is shown in Fig. S6, ESI†. **(a)** Selectively exciting the PtTPBP chromophores at 633 nm results in emission from upconverted α-6T singlet excitons. **(b)** Excitation at 405 nm results in emission from directly excited α-6T singlet excitons. **(c)** The PL spectra in **(a)** and **(b)** are integrated from **λ =** 500-600 nm and plotted as a function of incident power density. Trendlines with slope 1 and 2 are shown.

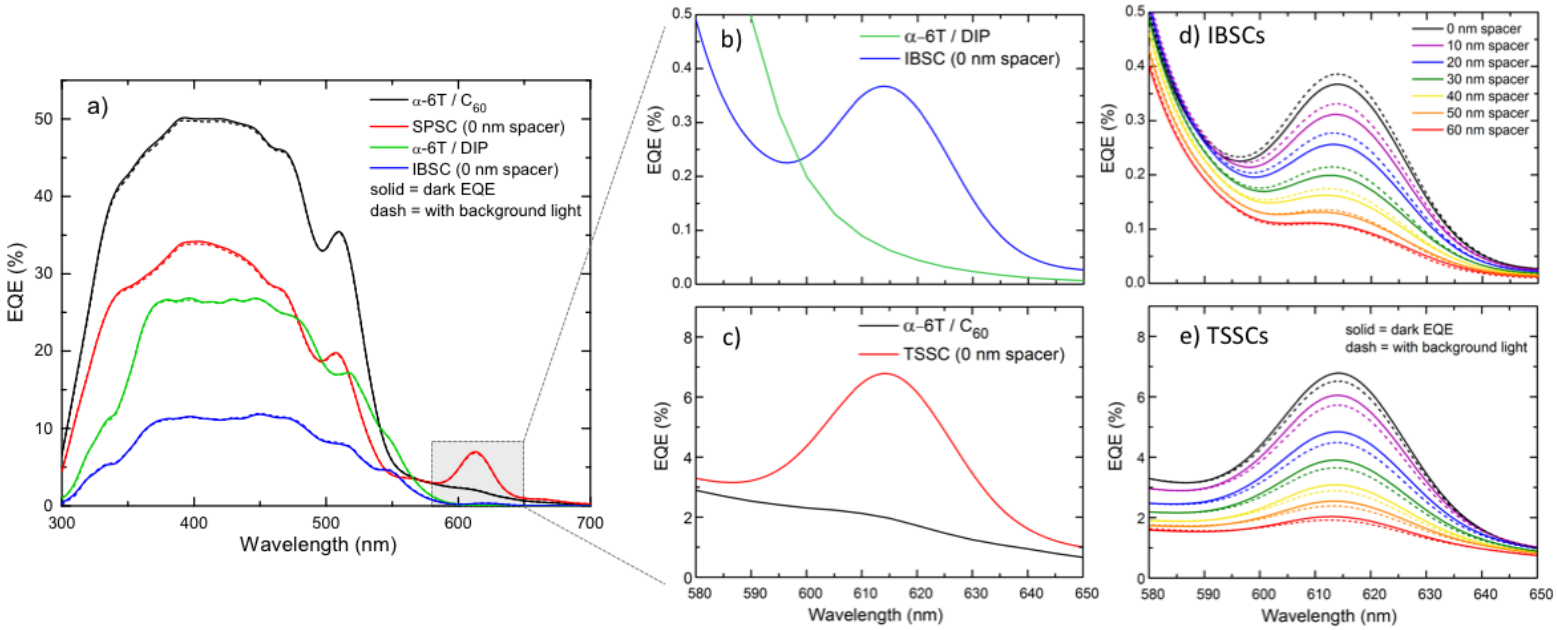

Figure 4. (a) Full EQE spectra of select devices with and without background white light. Detailed scans (measured without background light) of the **(b)** intermediate band solar cell (IBSC) and **(c)** triplet sensitized solar cell (TSSC) in the region of PtTPBP absorption, showing new sub-bandgap contributions to photocurrent that are absent in the unsensitized devices. EQE spectra around 615 nm in the presence of a background white light for select **(d)** IBSC and **(e)** TSSC devices. For the measurements performed under background white light (dashed lines), the incident power density was 0.19 mW/cm^2 for the IBSC and 0.54 mW/cm^2 for the TSSC. Curves represent spline interpolations.

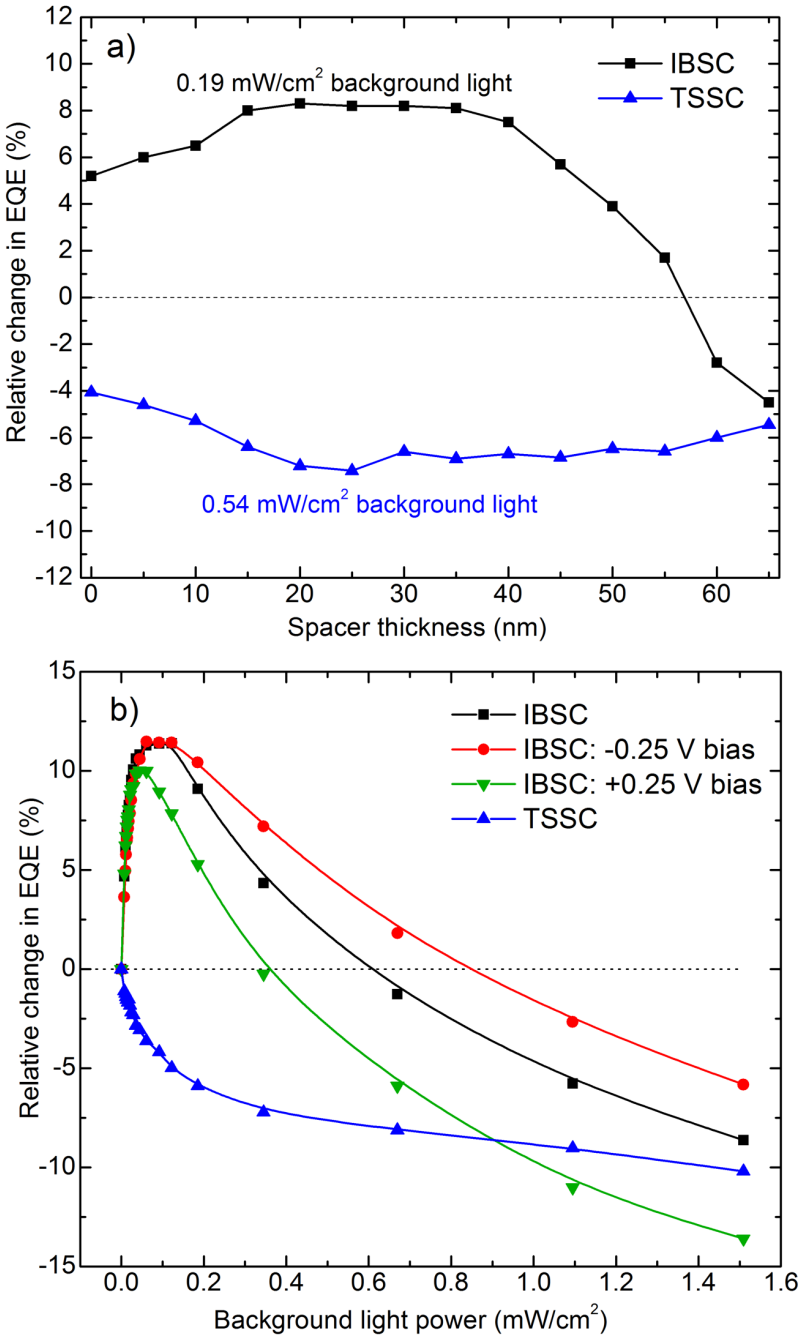

Figure 5. Response of the intermediate band solar cell (IBSC) and triplet sensitized solar cell (TSSC) under selective excitation of the PtTPBP with 615 nm light. **(a)** Percentage change in 615 nm EQE response under background white light as a function of α-6T spacer thickness. **(b)** Percentage change in 615 nm EQE response of the IBSC with a 20 nm α-6T spacer and TSSC with a 25 nm α-6T spacer as a function of background white light intensity. The response of the IBSC

under forward (0.25 V) and reverse (-0.25 V) voltage biases are also shown. Refer to **Methods** for full experimental details.